DEVELOPMENT OF A SINGLE-STAGE NANO INDENTER

BY

ALLEN GABRIEL CHARLES FERNANDES

THESIS

Submitted in partial fulfillment of the requirements
for the degree of Master of Science in Mechanical Engineering
in the Graduate College of the
University of Illinois at Urbana-Champaign, 2018

Urbana, Illinois

Adviser:

Professor Placid M. Ferreira

ABSTRACT

The current work seeks to understand the functionality of a single degree-of-freedom stage in a MEMS (Micro-Electromechanical system) platform that enables very precise displacement as well as force control. This type of stage finds use in determining fluid properties such as viscosity; to determine the strength and rigidity of carbon nanotubes (CNTs) and monolayers of graphene and for mechano-transduction in cellular mechanics and extracellular matrix. The current design is shown to produce a displacement of 39 μm and is capable of applying a theoretical maximum force of 260 μN. The study explores in detail the testing and analysis of the device without delving into great detail about the initial design and fabrication of the device itself. Much work was done to properly interface this MEMS device to the external world using connectors and a signal processing circuit in a custom-built PCB for improved noise reduction and enhanced signal strength. A capacitance-to-digital converter (CDC) IC, AD7747 is used for reading the capacitance signals from the MEMS device. The AD7747 uses I^2C communication protocol and Arduino ATmega 2560 was used to read the data generated by the IC. Moreover, image processing techniques were employed to track displacements down to 1 μm. The data from the image processing analysis along with data from AD7747 was used to characterize the devices for change in capacitance and displacement with respect to applied DC voltage.

ACKNOWLEDGEMENTS

I want to thank Prof. Placid M. Ferreira for his guidance and mentorship throughout my research here at the University of Illinois Urbana-Champaign. I would like to extend my gratitude to Ping-Ju Chen for partnering with me in this project and for her constant support.

Special thanks to Glennys A. Mensing, Laboratory Coordinator, MNMS cleanroom and Joseph Walter Maduzia, Laboratory Specialist, MNMS Cleanroom for their constant support.

Most of all this work would not be possible without the endless love and encouragement of my family and friends. Lastly, I want to thank God for his grace and mercy throughout the course of this research.

CONTENTS

CHAPTER 1 INTRODUCTION **1**

CHAPTER 2 DESIGN & FABRICATION **3**

CHAPTER 3 EXPERIMENTAL SETUP **7**

3.1 AD7747 7

3.2 ACF CONDUCTIVE FILM 8

3.3 SIGNAL PROCESSING BOARD 9

CHAPTER 4 TESTING & ANALYSIS **11**

4.1 TRIAL # 1 11

4.1.1 TROUBLESHOOTING 12

4.1.2 MODIFICATION TO RECIPE 15

4.2 TRIAL #2 16

4.2.1 CHARACTERISTIC CURVES 16

4.2.2 INFERENCE 22

CHAPTER 5 CONCLUSION **24**

REFERENCES 25

CHAPTER 1 INTRODUCTION

Micro/Nano stages capable of producing very accurate and controlled force (or displacement) output is essential in several different applications like optical switches, scanning probe microscopy, atomic force microscopy and imaging and data storage. Moreover, such technology also finds application in assessing the strength of (CNTs) Carbon Nanotubes and thin films such as monolayers of graphene. These require small forces that have to be applied in a controlled manner for understanding their behavior and response to the applied external force. Biological samples such as cells and tissues can be probed to understand their response to external force field. This is essential to having a clear understanding of the role of mechano-transduction in relaying important information through the organism. Furthermore, to understand certain fluid properties like viscosity and surface tension, ability to apply small forces is highly desired. Thus we see that a micro/ nano stage capable of generating small forces is plays a key role in advancing micro/nano science.

A MEMS (Micro- Electro Mechanical System) device with a small form factor can provide the desired range of displacement and force with a good bandwidth. Several research groups have made significant advancement in measuring small forces using MEMS technology. Kenny et al. [1] provides an instructive starting point for MEMS- based force measuring devices, analyzing different measurement approaches such as optical, piezoresistive, tunneling current, magnetomotive and capacitive sensing for their fundamental limits and confounding effects. Gnerlich et al. [2] have developed a piezoresistive MEMS force sensor for studying the cell biomechanics. Rajagopalan et al. [3,4] developed a MEMS force sensor to understand

the mechanical response of drosophila axons using flexible cantilever beams with probe tips attached to their ends. It has a resolution of 50 – 500 pN and a range of 100 nN – 1 μN. Bonjin et al. [5] developed a single stage MEMS device with a maximum displacement of 40 μm at 100 V using comb drive actuators. Dong et al. [6] developed a two-dimensional micro stage using parallel kinematics and comb actuators that is capable of 20 μm displacement at 100 V without any parasitic motion in the lateral direction. The current works seeks to interface and characterize a single stage MEMS device to be used for probing biological samples.

CHAPTER 2 DESIGN & FABRICATION

The design presented here is similar to the ones published earlier by our group [5, 6, and 7] and the same design principles have been applied for this study. For a more detailed understanding of the design methodology the reader is directed to work previously done by our group. There are two pairs of combs - one for the sensing side and the other for the actuation side. The sensing and actuation sides are coupled with each other mechanically i.e. they move in conjunction with each other, but they are decoupled electrically. Figure 2.1 shows the key features in the design of the MEMS device. It is essential to decouple the two sides electrically because they operate at different voltage levels. The sensing side operates at 5 V whereas the actuation side operates at 100 V. Therefore, this difference in the operation voltage can easily lead to cross-talk and noise in the output signal. SOI wafers with 50 μm device layer, 500 μm handle layer and 2 μm buried oxide (BOX) layer was used to fabricate these devices. The sensing comb has a differential arrangement, designed to take maximum advantage of the measuring range of the CDC (Capacitance to Digital Conversion) IC – AD7747. Therefore, motion of the probe will increase the finger overlap (and hence, capacitance) for one comb while it decreases for the other comb. There are 188 fingers in one comb, 156 fingers in the other comb and a finger height of 50 μm for both combs. The spacing between the adjacent combs fingers is 5 μm – limited by our process. The initial overlap between the moving and stationary fingers for two combs are 50 μm and 10 μm respectively (this asymmetry is used because motion of the probe decreases the overlap of the first comb while increasing that of the second). The differential comb set-up should theoretically produce a capacitance change rate, $\Delta C/\Delta x$, of 0.0610 pF/ μm (since there are two sets of differential capacitive combs), with air being the medium between the comb fingers.

The actuation combs and leaf springs are designed in a similar iterative manner. Folded beam springs are used for suspending the probe instead of doubly supported beams because they

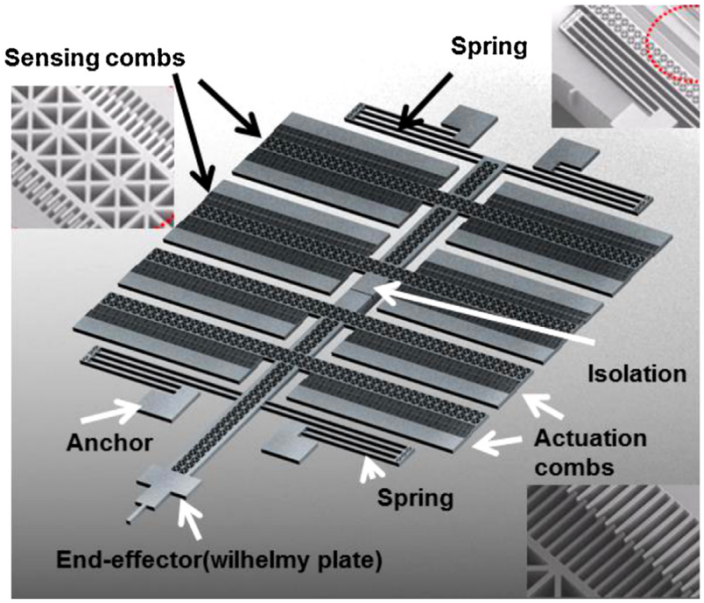


Figure 2.1 Solid model of the probe with key parts. SEMs of important features; courtesy: Bonjin et al. [5]

offer a larger linear (constant stiffness) range of motion. The designed springs have a theoretical stiffness of 6.65 N/m. Therefore, given a position resolution in the range of 1-5 nm, the probe is expected to have a theoretical force output of 6.65 – 33.25 N/m. Thus the major design constraint when designing the actuator combs was to overcome the spring stiffness. The combs are designed with 188 fingers with a height of 50 µm and gap of 5 µm such that the electrostatic force is sufficient to produce the desired displacement at a given maximum actuation voltage. The theoretical electrostatic force, F_e is 310 N at 100 V using the following well-known equation for comb drives.

$$F = n.\epsilon o.h.\frac{V^2}{g}$$

This force will produce a displacement of 40 µm with the designed spring stiffness. For an amplifier with 10 mV resolution, the probe will be capable of exerting a force with a resolution of 30 nN.

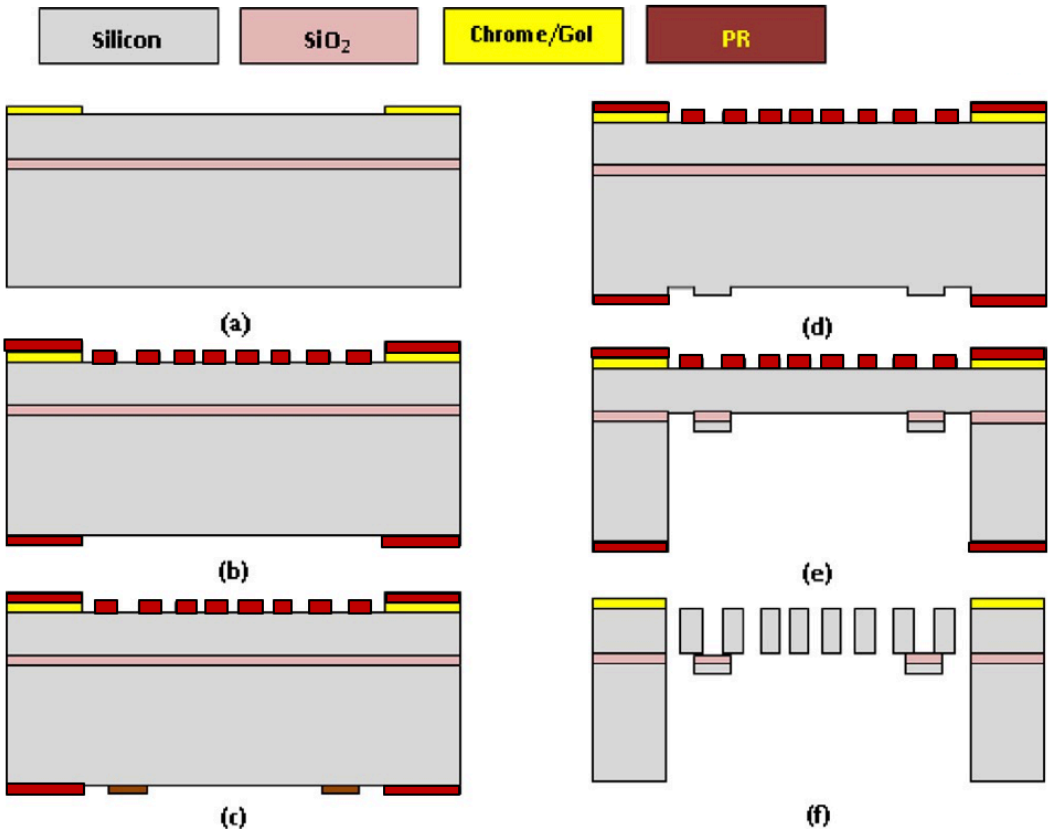


Figure 2.2 shows the process flow. (a) pattern and deposit contact pads; (b) Pattern device side with all the features; (c) Pattern the bottom side to make the electrical isolation pads; (d) DRIE etch backside to create the etch profile for making electrical isolation pads; (e) DRIE etch the handle layer followed by HF etch to remove buried oxide layer; (f) DRIE etch topside to create the device features

The overall fabrication procedure for the MEMS probe is very similar to that reported by our research group for fabrication multi- axis MEMS positioning stages [24, 25] and is summarized in Fig. 2.2. The device is fabricated as 15 mm x 15 mm die on a SOI wafer with 500 µm handle layer and p – doped 50 µm device layer. There are 2 topside patterning and 2 bottom side patterning

steps followed by HF etch to remove the BOX layer. The first topside mask is used to pattern and etch the contact pads in the device. The second topside mask creates the fingers and all the device features on the 50 μm device layer. The bottom side (handle layer) is next patterned to make the electrical isolation pad. The etching is first done on the bottom side followed by an oxide etch to remove the BOX layer. The final step is to etch the device layer on the top to release the features.

CHAPTER 3 EXPERIMENTAL SETUP

The experimental setup for characterizing the MEMS device is shown in figure 3.1. In order to run the experiment, there are several components that need to be properly interfaced and programmed. The following sections discuss the various issues encountered in interfacing the MEMS device.

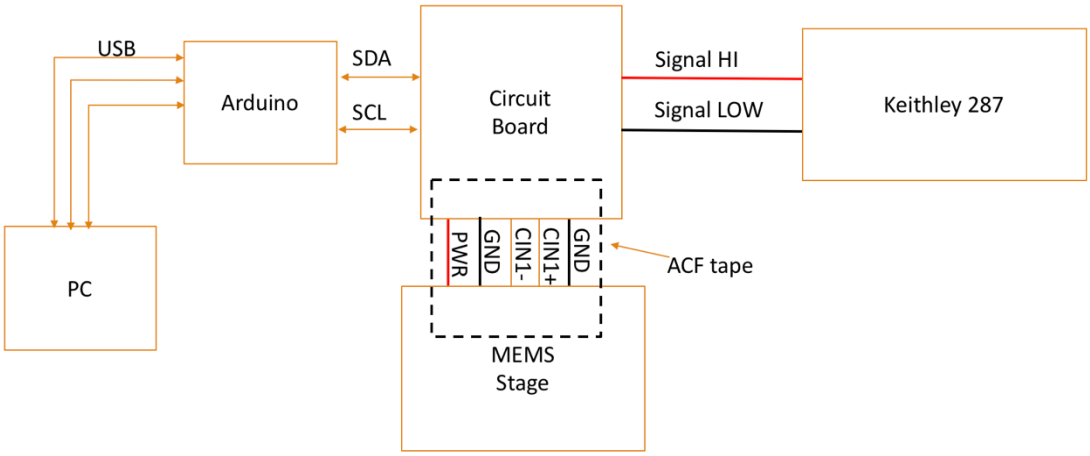


Figure 3.1 Connection schematic for characterization experiments

3.1 AD7747

The AD7747 is a capacitance-to-digital converter IC which is used to convert the change in capacitance to a voltage signal between 0-5V. The differential comb set-up should theoretically produce a capacitance change rate $\Delta C/ \Delta x$, of 0.0610 pF/ µm. Therefore, the IC is chosen such that it has a linear range that falls within the specified device limit. AD7747 has a normal mode range of ±8.192 pF and it has a 24-bit conversion efficiency which puts the resolution to 31.25 aF. It uses I^2C serial communication protocol and ATmega 2560, board is used to interface the IC with the computer.

The I^2C interface meant that there are two lines SDA and SCL to interface with the AD7747. The architecture of the board uses three 1-byte (8 bits) registers to store the capacitance value.

The first register indicates a completed conversion. The next three registers store the cap data. Reading the data from these registers was a major issue during the initial phase because the registers have an inherent feature wherein they have to be read continuously one after the other in sequence always starting from the first register. Since the first register does not give out the cap data, any attempt to start from register 2 will end in giving an incorrect reading because defaulted to reading from the first register. So after debugging the code, the final solution to this was to read all the four registers but skip the first register's value and then proceed to assemble the remaining three registers.

3.2 ACF conductive film

After the IC was fixed, the next issue to be addressed was interfacing the MEMS Device with the external circuitry. This required the use of Anisotropic Conductive Film which has conductive silver particles embedded in a polymer substrate. Upon application of heat and pressure the conductive particles line up and form a continuous trace which provides the current path between the device and external circuit.



Figure 3.2 Soldering iron with aluminum insert for ACF bonding

The ACF film required uniform heating at around 160 F and pressure of 30 psi for 30 s and then allowed to cool at room temperature for 30 s. This process is critical, and it ensures that a good bond is formed between the silicon surface and conductive particles. Initial trials proved ineffective because of higher temperature setting and non-uniform heating. A simple experiment

was performed by varying the temperature to optimize the temperature setting as seen from table 3.1. The heating element was a soldering iron with an aluminum insert shown in figure 3.2 and it was used to apply uniform heat. The pressure setting was not carefully controlled as it did not have a significant impact in the quality of the bond.

Table 3.1 Temperature setting for optimal ACF bonding

S.No	Temperature (F)	Time	Result
1.	460	30 s	Over burn
2.	360	30 s	Poor adhesion
3.	420	30 s	Good adhesion

3.3 Signal Processing Board

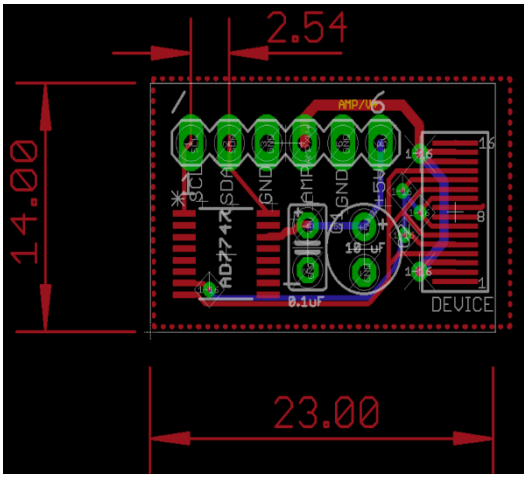


Figure 3.3 PCB design in Autodesk Eagle - version1

The use of breadboard to interface the different components with each other resulted in noise and EMI which reduced the signal-to-noise ratio significantly. Thus, it was decided to custom-make a circuit board that would encompass all the necessary traces to interface with the different components. Autodesk Eagle was used to design the circuit board (see figure 3.3). The main goal was to limit the space that the board would occupy. This will make the device more portable and versatile for multiple

applications where space is a major constraint. The first version of the board was found to be too small, which was advantageous in that it took up very little space. But it lacked rigidity and would topple up under the slightest jerk. Therefore, it was decided to design another version which was slightly bigger and sturdy. The result is the design shown in figure 3.4 that highlights all the major changes made to this board. It has more connection points for connecting the power source and I^2C ports. Another feature to note is that the board contains the traces to the ACF pads with the device sitting inside the board itself. This would ensure the device is well grounded and all ground-loops are eliminated.

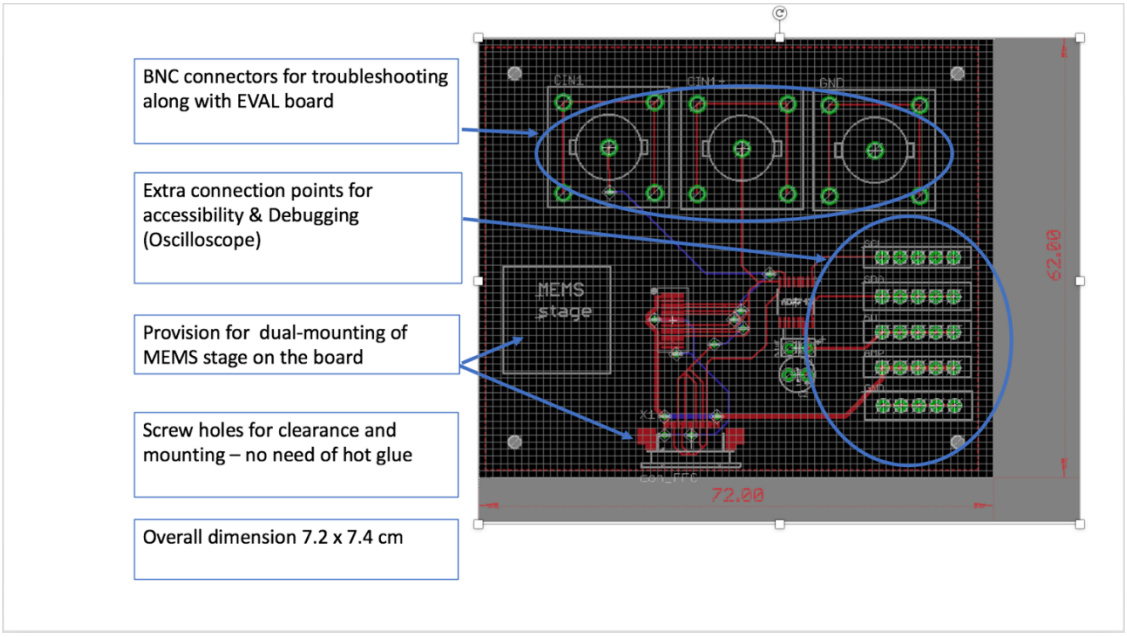


Figure 3.4 PCB design highlighting major improvements made in version 2

CHAPTER 4 TESTING & ANALYSIS

The experimental setup (see figure 4.1 & 4.2) was now complete and all the required components for running the experiment were properly interfaced. The testing and analysis was done in MNMS (Micro-Nano Mechanical System) cleanroom. The displacement of the probe tip was captured under a high-power microscope with 100x magnification. The Keithley 256 was used for providing the constant voltage to actuate the comb drives and the custom-built PCB was used to interface the AD7747 and Arduino with the MEMS Device.

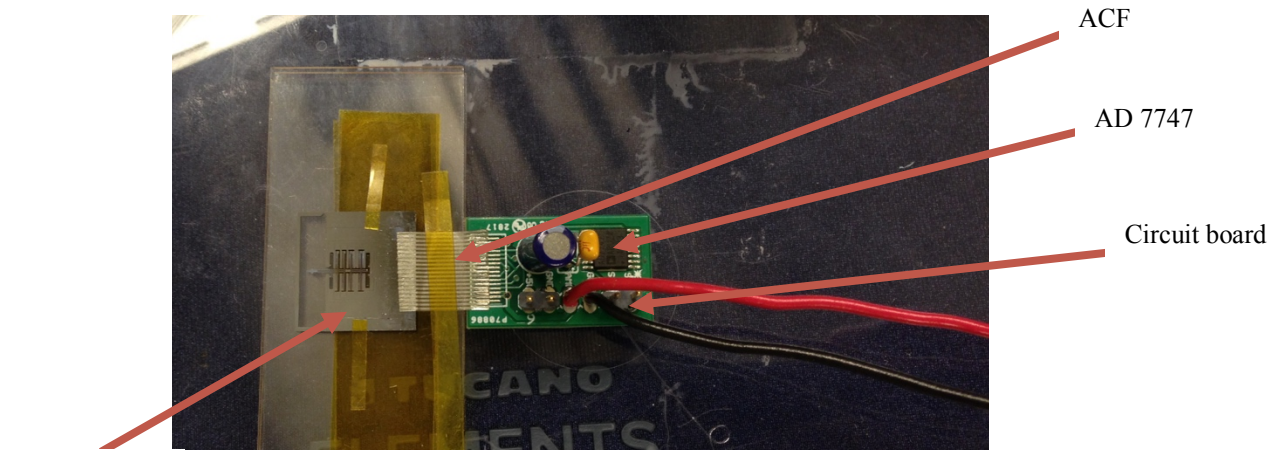


Figure 4.1 Test setup showing the MEMS device, circuit board with all the connections

4.1 Trial # 1

The first trial proved ineffective to produce any significant displacement. There was some negligible amount of motion, but it was firstly, very small. Secondly, it was angled -the probe moved at an angle. Thirdly, the Keithley power source gave an error message – 'Compliance' - for voltages greater than 10 V indicating that the device was drawing more current that it should. Lastly, a close look at the ACF bonding site showed imperfect alignment. The

following section addresses these challenges and provides the method adopted for troubleshooting these different errors.

4.1.1 Troubleshooting

a. *Pitch mismatch*

The first problem identified when troubleshooting the test setup was that there was a misalignment in the ACF bonding. It was later identified that there was a 20 µm mismatch between the pitch of the ACF tape and ACF trace in the PCB. This was clearly a human error and the problem was not evident because there are 16 circuits in the ACF connection and only the last few circuits had the mismatch reflected in their alignment. The 20 µm error accumulated causing the later circuits to be offset with respect to each other.

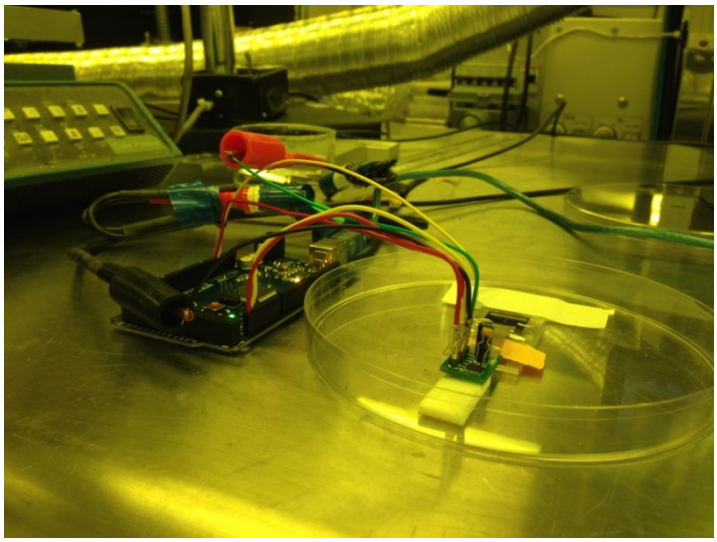


Figure 4.2 Test setup with all connections

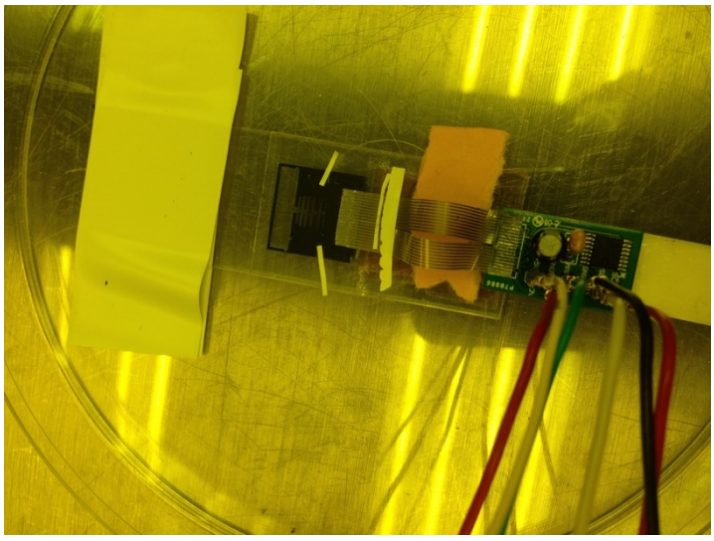


Figure 4.3 Test setup with ACF split in half to overcome pitch mismatch

The proper way to resolve this issue is to make changes to the pitch in the PCB and then re-print the board. But keeping in mind

the time constraint a rather crude but effective method to temporarily resolve this issue was used. The 2 cm long ACF tape was slit in the middle as shown in figure 4.3 and as a result the ACF tape instead of being one single strand became two separate strands. This temporarily fixed the problem and allowed the continuous testing of the device.

Further preliminary testing resulted in a straight line motion and thus it became evident that the angular displacement of the probe tip was probably because of the pitch mismatch. This makes sense because if the circuits were not properly connected to each other which implies that they were not receiving power on both ends which ultimately means that only one of the two sides of the device was powered. This explains the angular motion of the device.

b. Compliance error

The compliance error was the next most puzzling issue in the whole testing process. By definition, compliance as used in electrical test equipment, refers to a safety feature that prevents the device under test (DUT) from drawing current greater than a threshold value. This is a safety feature that shuts-off the voltage source when the DUT is drawing excessive current.

In theory, a series of parallel plates arranged in a comb fashion is basically a capacitive unit. In the ideal case there should be no current flow in the circuit except for very small displacement current due to the capacitive action. Thus, the whole notion of compliance has no meaning when dealing with comb drives unless there is a short somewhere in the circuit.

The following procedure was used to troubleshoot the system for compliance and it was used to identify and pinpoint the source of this error. First thing to note is that there are only 3 main components involved in the system:

1. The Keithley power source
2. The PCB with connectors
3. The MEMS Device

The first step was to check if the power source. This is important because a malfunctioning unit might give error messages even when everything is working fine. The easiest way to check the power source was to switch out the power supply with another one and run the same experiment again. This resulted in the same error message which proved that the power source was indeed working fine.

The next thing in line was the custom-built PCB with its different connectors and circuits. The PCB was checked using digital multimeter for connectivity and shorting. The files were also carefully examined to inspect for any shortage. And everything seemed to be working fine. This ruled out the next possibility of error. That only leaves the MEMS device and it was next in-line to be inspected for defects.

The MEMS device was checked under the microscope thoroughly for any form of defect or shorting. The device looked perfect under the microscope and it showed no sign of defect. A closer look revealed something that looked like black debris or dirt underneath the comb tips. This initially was assumed to be dust sticking to the glass slide. But a careful inspection of the rear side of the comb drive showed thick chunks of silicon still left unetched and was sticking to the tip of the comb fingers (see figure 4.4). Finally, it is clear what was causing the compliance error. The fingers were supposed to be etched clear all the way through leaving nothing in between them, But the presence of these thick silicon blobs underneath the fingers meant that the stationary and moving comb fingers cannot freely slide in and out of each other.

In the beginning they start to move and there is no sorting but then once the fingers make contact with the unetched silicon, the short out and the equipment outputs ‘compliance’ error message.

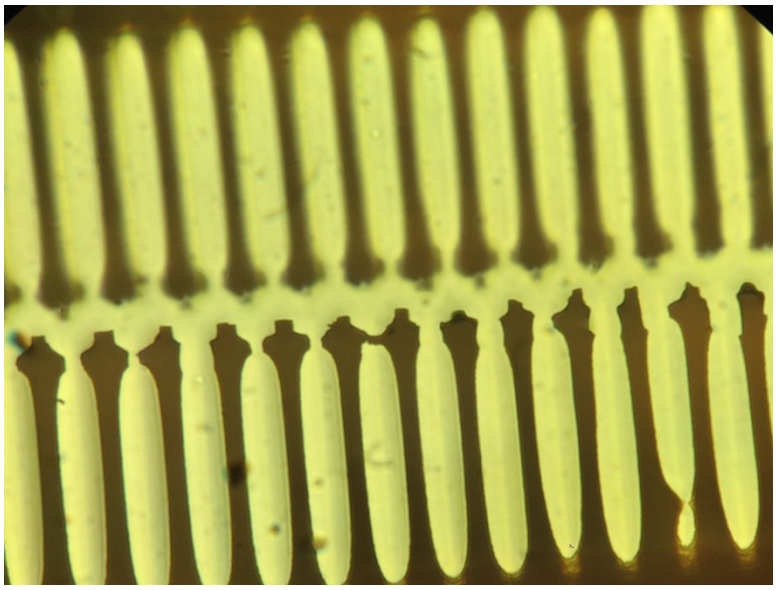


Figure 4.4 Image showing incomplete etch of comb fingers using bottom-side illumination; darker region shows the comb fingers

4.1.2 Modification to recipe

The problems noted in the first trial were clearly traced back to the root cause. Now the root cause for these problems had to be rectified. One major problem is that of incomplete etch and this was resolved using a slight change to the process flow for fabricating these devices. The original recipe involved the bottom side to be etched first using DRIE and then the buried oxide layer was etched using HF and lastly a topside etch to release the comb fingers. However, this proved ineffective to completely etch the silicon in between the fingers. Thus, a modification to first etch the topside using DRIE and then a HF etch to remove the buried oxide layer followed by another DRIE to etch the bottom side. This will ensure that the space between the fingers is traversed twice – first from topside and then from bottom side. This technique effectively eliminated the incomplete etch problem.

4.2 Trial #2

The second trial was performed using a new batch of devices fabricated using the modified recipe and the following characteristic curves were obtained.

4.2.1 Characteristic curves

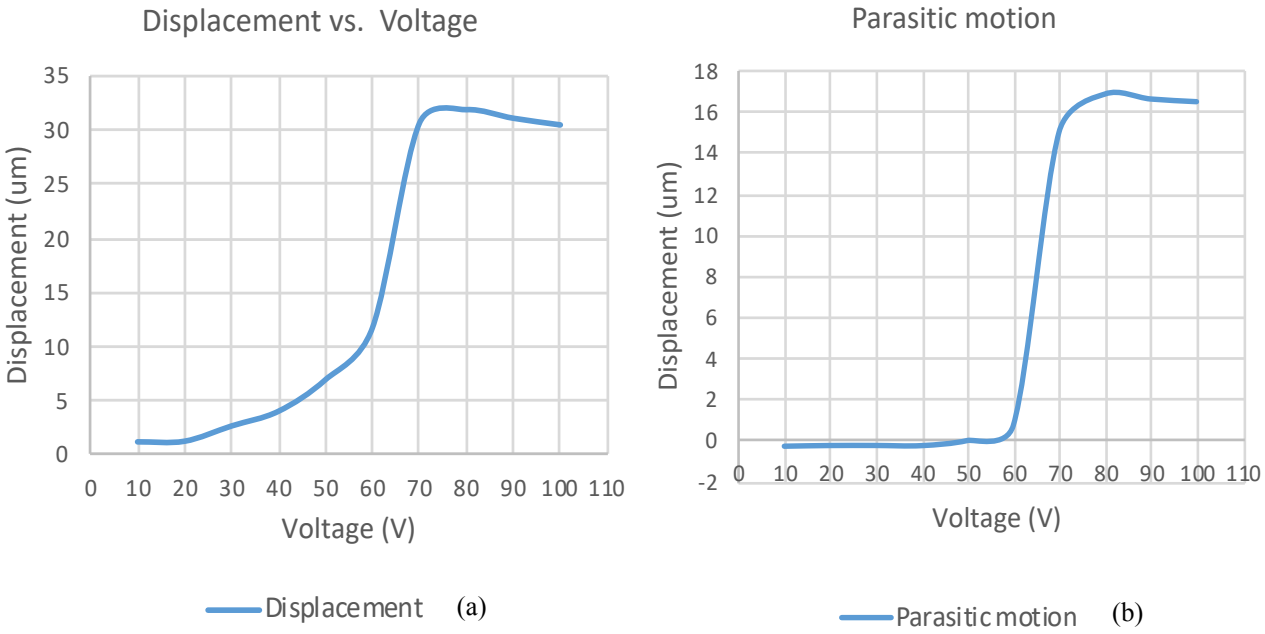
The Displacement vs. Voltage curves were obtained using the image processing data. The probe was connected to the CV (constant voltage) power source and its displacement was observed under a high-power Olympus microscope at 100x zoom. The voltage was increased in steps of 10 V and the displacement at each voltage step was captured. These images were then complied into one movie using Tracker, which is a free software for making image analysis. Then using a technique called Digital Image Correlation (DIC) the images are checked for a particular feature and the position of the feature relative to a reference image is obtained. This method can be used to track features in the sequence of images using the first image as a reference.

a. Displacement vs. Voltage - sample 1

The first sample that was tested gave the following test results. Graph 4.1(a) shows the displacement in the desired diredction of motion and graph 4.1(b) shows the displacement in the lateral direction (parasitic motion). Graph 1 showing motion in the desired direction has the expected parabolic shape which is inline with the square dependence of displacment with voltage. There are several other interesting inferences that can be drawn from these graphs and they are discussed briefly in the following sections.

Breakdown

The device breaksdown and goes unstable at ~70 V and any further increase in voltage does not lead to an increase in displacement. The displacement is 30. 775 µm for 70V. This is 35% more



Graph 4.1(a) Plot of displacement vs. voltage in the desired direction; Graph 4.1(b) Plot of displacement vs. voltage in the lateral direction (Parasitic motion)

than the theoretical 22.8 µm. Therefore it is clear that the device moved farther than it should have which maybe due to the premature failure of the mechanical joint which is addressed in the following sections.

Parasitic Motion

The is parasitic motion is approximately zero for volatages less than 60 V but it shoots up to a staggering 16 µm for 70 V. This is highly undesirable because one of the primary advantages of comb drive is a guaranteed straignt line motion. Parasitic motion can and in most cases will lead to a permanent damage. As the gap between two adjacent comb fingers is only 5 µm , any lateral displacement of 5 µm or greater implies a contact between adjacent comb fingers and potential

shorting. This is evidenced from the fact that post – test analysis of the device shows broken comb fingers which may be a result of the moving comb travelling in an angular motion (see figure 4.5 (b)).

Mechanical Joint failure

The mechanical lap joint between the actuation and sensing sides gave in. This was evident from the post-processing image- figure 4.5 (a). It is unclear whether the lateral displacement caused the mechanical joint to rupture or if the failure of the mechanical joint caused the lateral displacement. The failure of the joint may also be due to over-etching of the silicon oxide layer during the HF etch process. Thus it is unclear as to how to address this problem.

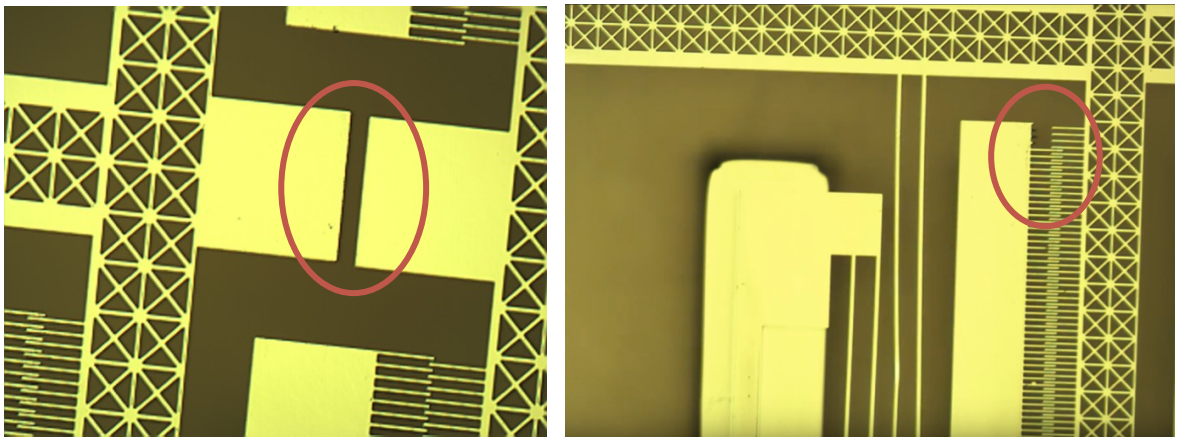
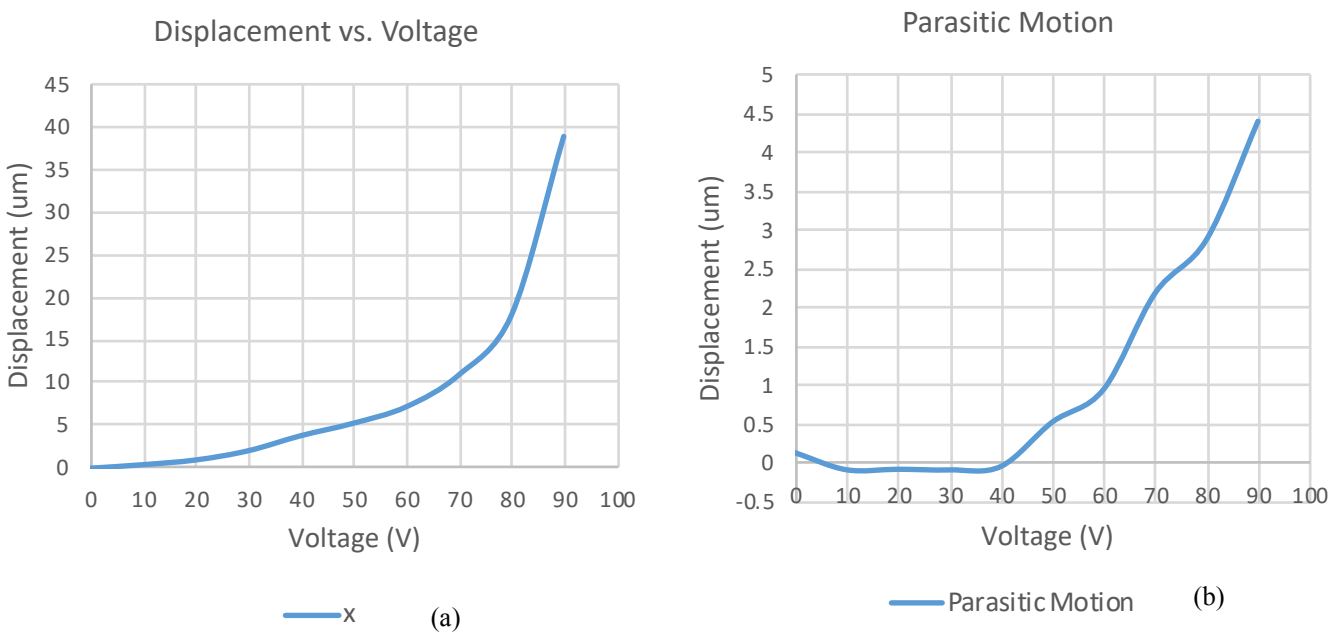


Figure 4.5(a) Mechanical joint failure during testing for sample 2; Figure 4.5(b) Damaged combs indicating contact between adjacent fingers

b. *Displacement vs. Voltage - Sample 2*

The following graphs are showing the displacement data for a second sample that was tested. Graph 4.2(a) shows the displacement in the desired diredction of motion and graph 4.2(b) shows the displacement in the lateral direction (parasitic motion). The displacement in the desired direction has the expected parabolic shape. The main inferences drawn from these graphs are summarized in the following sections.

Breakdown

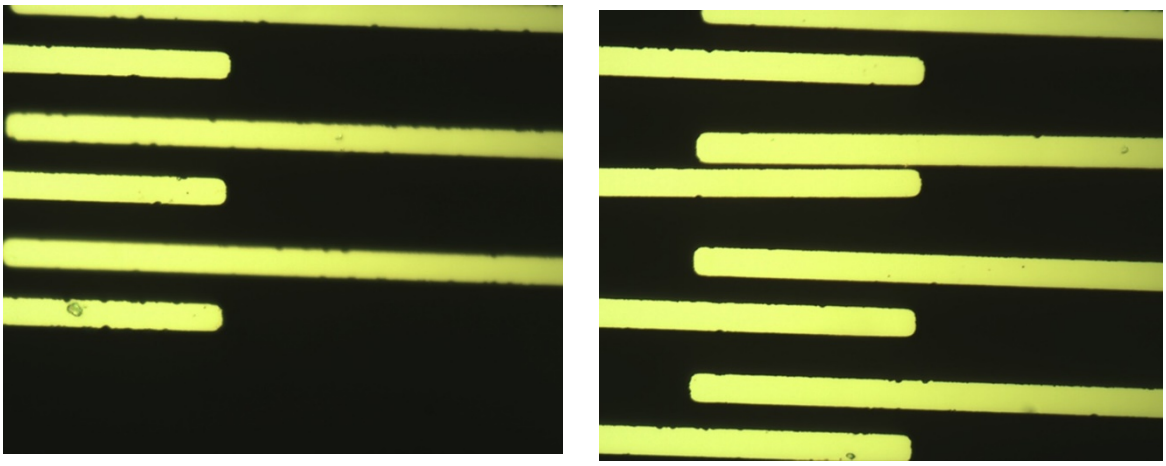


Graph 4.2(a) Plot of displacement vs. voltage in the desired direction; Graph 4.2(b) Plot of displacement vs. voltage in the lateral direction (Parasitic motion)

The data shows a maximµm displacement of 40 µm at 90 V. The shape of graph 4.2(a) is parabolic. The device brokedown at 90V and the power supply reported 'compliance' at 90 V.

Parasitic motion

The lateral displacement is approximately zero below 40 V. It then begins to climb and follows a parabolic shape. At 90 V, it hits a peak of 4.5 µm . This means that the comb fingers probably made contact with each other since the gap between adjacent combs is 5 µm . This is evident from post-test analysis of the sample as seen in figure 4.6. The power supply also reported 'compliance' which further proves the fact hat the comb fingers made contact.

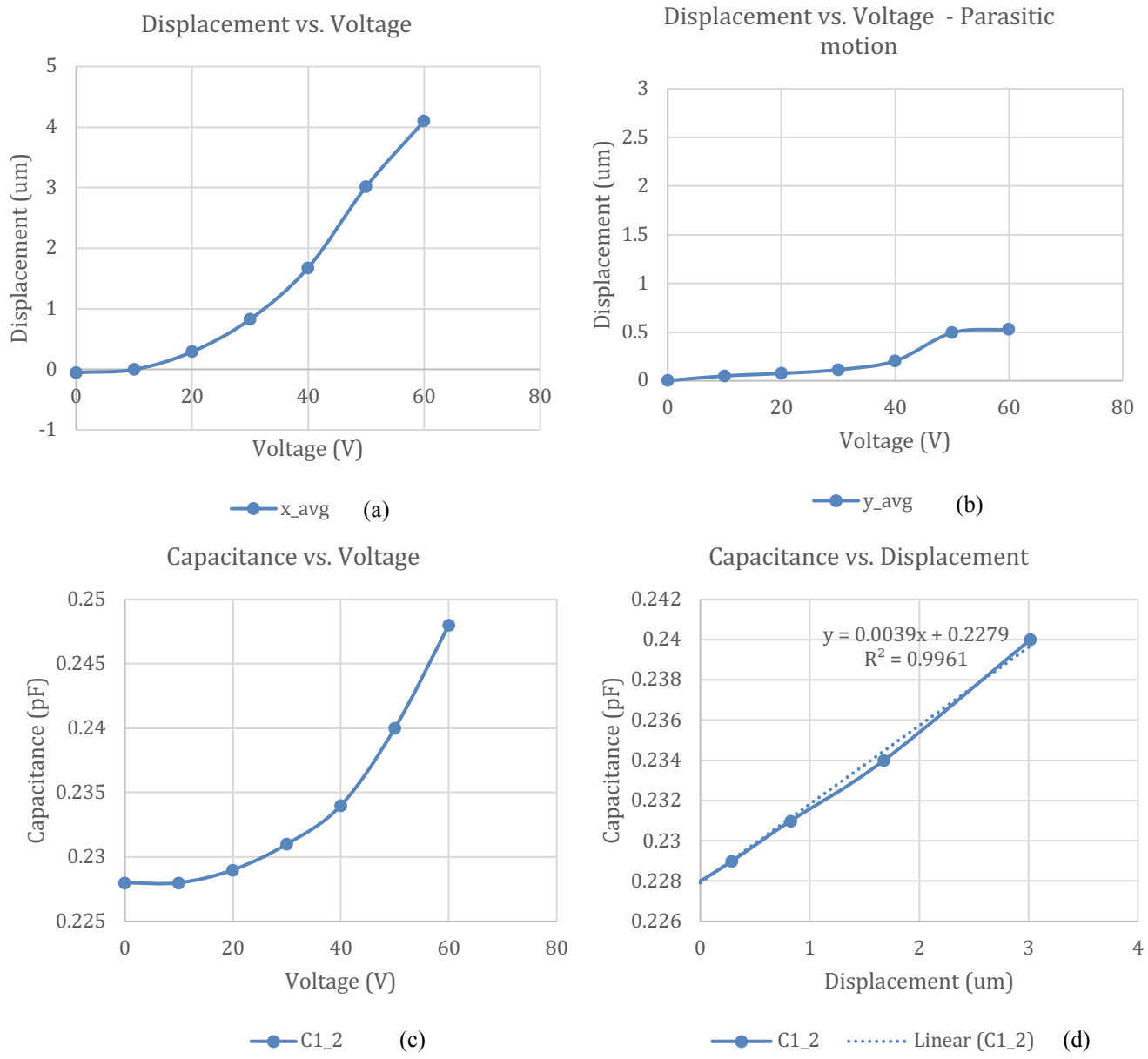


(a) (b)

Figure 4.6 (a) Shows the comb fingers before testing and (b) shows the combs making contact with each other after testing

c. *Characterization results – Sample 3*

The following sample was tested under the exact same conditions and the graphs 4.3 were obtained. Graph 4.3 (a) shows the displacement in the desired diredction of motion and has the expected parabolic shape. It is essential to note that the device was energized to a maximum of 70 V. Graph 4.3(b) shows the displacement in the lateral direction (parasitic motion) and is it remains faily low even at 70 V . The testing was limited to 70 V inorder to preserve the device from permanent failure due to mechanical joint failure or any excessive parasitic motion. This enabled us to conduct further testing with the device and has helped retain the device. Thus, it was used for making electrical characterization. The device was energized and its change in capacitance was detected using the AD7747. This data is shown in graph 4.3(c). The graph also has a parabolic relation and this is expected as $C \propto V^2$. Lastly, graph 4.3(d) shows the linear relationship between the change in capacitance (ΔC) and displacement in the desired direction (Δx). The main inferences drawn from these graphs are summarized in the following sections.



Graph 4.3(a) shows the plot of displacement vs. voltage in the desired direction; 3(b) shows the plot of displacement vs. voltage in the lateral direction (parasitic motion); 3(c) plot of capacitance vs. voltage as read from AD7747; 3(d) plot of capacitance vs. displacement

Displacement

The displacement is much less than the expected value. It is unclear at this stage as to why the displacement is low because the voltage was limited to 60 V. From the data we have a maximum of 4.1 µm at 60 V. This value is 4 times less than the theoretical value of 16.8 µm. From graph

4.3(d), the ΔC/ Δx is 0.0039 pF/ μm which is an order of magnitude less than the theoretical 0.0610 pF/ μm. The exact reason for the difference is unknown and more testing is necessary to understand this phenomenon.

Parasitic motion

The device has a fairly good performance when considering the parasitic motion. The maximμm parasitic motion is less than 0.5 μm at 60 V. We do not know if there is an increasing trend because we do not have the data to make any claims. However, for the test cycle the parasitic motion was 0.5 um or less.

4.2.2 Inference

a. *Large parasitic motion*

Now from these data samples one of main problems that remains to be addressed is the large parasitic motion. There are several possible explanations that may explain this effect, but it is unclear at this point as to the exact cause of this effect. Firstly, there is a chance that the ACF that connects the power supply to the MEMS device may not have bonded equally on both sides. This would cause disproportional voltage being supplied to the two ends of the device. As a result, the device would experience a torque or twist and the displacement will not be a pure rectilinear motion. Secondly, there exists the possibility that the two suspended beam flexures are not equally etched. Therefore, the device may be inclined to move towards one side of the device causing a rotational twist which increases in degree as the voltage is increased. Lastly, the twist in the motion can also be a byproduct of residual stress build up in the device during the removal of the buried oxide layer using HF. This residual stress may reflect itself as a bow or dup in the overall topography of the device layer causing unusual behavior. These are just different hypothesis that

explain the parasitic behavior of the device and it remains to be tested which (or any) of these accurately explain the lateral motion.

b. *Mechanical joint failure*

Unlike the parasitic motion which remains to be properly explained, the failure of the mechanical joint can be fairly accurately attributed to over-etching of the lap joint during the final removal of the oxide layer using HF. This causes undercut in the oxide pad which reduces its effectiveness to hold the two-halves of the device together at higher voltages. The solution to this effect will be to optimize the etch time for removing the buried oxide layer as this would prevent undercut of the lap joint. Second measure that can prevent this effect will be to increase the size of the lap joint itself. That way even if there is an undercut it will not be significant enough to cause a catastrophic failure. Again, it remains to be verified if either of these solutions will effectively tackle the problem of mechanical joint failure.

CHAPTER 5 CONCLUSION

The current work demonstrates the functionality of a single degree-of-freedom stage in a MEMS (Micro-Electromechanical system) platform that enables very precise displacement as well as force control. The current design is shown to produce a displacement of 39 μm and is capable of applying a force of 350 μN. The study explores in detail the testing and analysis of the device with emphasis on proper interface of this MEMS device to the macro-world using appropriate connectors and a signal processing circuit in a custom-built PCB for improved noise reduction and enhanced signal strength. Basic image processing techniques were employed to study the device behavior and this data was used to characterize the device.

Therefore, the work is now partially completed in that the device is properly interfaced with all the necessary electronics and drive circuitry to actuate and sense the signals from the device. But, a lot of work needs to be done to optimize the process parameters for the device fabrication especially as it relates to the mechanical joint failure namely the etch time for removing the buried oxide layer. Further work is also needed to understand the exact cause for the parasitic motion and the solutions to address this effect. The reader is referred to the different hypothesis presented in the previous section and it is essential to clearly identify the cause and eliminate this effect for robustness and reliability of the device.

REFERENCES

[1] Kenny T. Nanometer-scale force sensing with MEMS devices. IEEE Sens J 2001;1(2):148–57.

[2] Gnerlich M, Perry SF, Tatic-Lucic S. A submersible piezoresistive MEMS lateral force sensor for a diagnostic biomechanics platform. Sens Actuators A: Phys 2012;188:111–9.

[3] Rajagopalan J, Tofangchi A, Saif MTA. Highly linear, ultra sensitive bio-MEMS force sensors with large force measurement range. In: Paper presented at the proceedings of the IEEE international conference on micro electro mechanical systems (MEMS). 2010. p. 88–91.

[4] Rajagopalan J, Saif MTA. MEMS sensors and microsystems for cell mechanobi- ology. J Micromech Microeng 2011;21(5).

[5] Bonjin Koo et al. An Active MEMS probe for fine position and force measurement, Precision Engineering 38 (2014) 738–748

[6] Dong J, Mukhopadhyay D, Ferreira PM. Design, fabrication and testing of a silicon-on-insulator (SOI) MEMS parallel kinematics XY stage. J Micromech Microeng 2007;17(6):1154–61

[7] Koo B, Zhang X, Dong J, Salapaka SM, Ferreira PM. A 2 degree-of-freedom SOI- MEMS translation stage with closed-loop positioning. J Microelectromech Syst 2012;21(1):13–22.